Daily Evapotranspiration Mapping using Regression Random Forest Models

Consuelo Gonzalo-Martín, Mario Lillo-Saavedra, Angel García-Pedrero, Octavio Lagos and Ernestina Menasalvas

Authors' version. Accepted for publication in the IEEE Journal of Selected Topics in Applied Earth Observation and Remote Sensing.
DOI: 10.1109/JSTARS.2017.2733958

***Abstract*—Efficient water management in agriculture requires an accurate estimation of evapotranspiration (ET). Even though local measurements can be used to estimate the components of the surface energy balance, these values cannot be extrapolated to large areas due to the heterogeneity and complexity of agricultural and natural land surfaces; and the dynamic nature of their heat processes. This extrapolation can be done by using satellite imagery, which provides information in the infrared thermal band; however, this band is not available in most current operational remote sensors. Our work hypothesis is that it is possible to generate a spatially distributed estimation of ET_d without thermal band by using non-parametric models as Regression Random Forest Models (RRFM). Six Landsat-7 scenes were used to generate the RRFM. Results were evaluated by comparing the values of ET_d provided by RRFM with that obtained using surface energy balance model. It has been shown than the results generated by RRFM present a good agreement with METRIC results, both quantitatively and qualitatively, especially for agricultural vegetation and forest land covers. Moreover, it has been detected that the RRFM estimation quality depends on the meteorological conditions on the days previous to the satellite register. It can be concluded that the ET_d estimated by the RRFM would be feasible for real applications when the thermal band it is not available.**

***Index Terms*—Evapotranspiration; Regression Random Forest; METRIC; Medium resolution satellite images; Remote Sensing.**

I. Introduction

It is well known that the demand for water is under growing pressure as the human population grows. Although this problem has been presented common throughout history, it is currently becoming more widespread and its impact more devastating. New threats include the climate change, which is likely to alter both water availability and water demand, in particular in agriculture [1]. In this scenario, it is clear that one of the main challenges of the 21^{st} Century is the increase in agricultural water productivity [2]. This situation has triggered the search for solutions to alleviate the differences between demand and supply in terms of water quantity, quality and timing. According to the FAO, agriculture uses approximately 70% of the world's freshwater supply [1]. Therefore, accurate information on agricultural water requirements is crucial for an efficient water management and productivity. One of the most extensively used way to evaluate these requirements is estimating evapotranspiration values (ET). ET represents the total amount of water lost via transpiration and evaporation from the canopy and soil in an area where crops are growing. ET at the land surface is considered as the most important process in the determination of the exchanges of energy and mass among hydrosphere, atmosphere and biosphere. However, measuring and modelling daily evapotranspiration (ET_d) is not straightforward due to the natural heterogeneity and complexity of agricultural and natural land surfaces. Several approaches have been proposed in the literature to estimate ET_d: i) a two-step approach by multiplying the weather-based reference evapotranspiration ET_r by crop coefficients (K_c) has been researched by several authors [3]–[5]. Crop coefficients are determined according to the *in-situ* type of crop and the crop growth stage [4]; ii) based on the Penman-Monteith (*P-M*) equation [6], with crop to crop differences represented by the use of specific values of surface and aerodynamic resistances [7]–[12]; iii) and other approaches extend the *P-M* single layer model to a multiple-layer model. A one-dimensional model of crop transpiration is combined with a one-dimensional model of soil evaporation in [13]. Unfortunately the aforementioned methodologies for modelling ET_d estimate latent heat fluxes locally and do not provide a spatially-distributed estimation.

Nowadays it is possible to estimate ET_d for different crops, providing spatial and temporarily distributed information over a wide area, using information gathered from aircraft or satellite platforms. Two methods for ET_d estimation from remote sensing data can be found in the literature: i) methods that use visible and near infrared sensors to extract a vegetation index (VI) and the surface radiative temperature to estimate its corresponding skin temperature [14]–[16] and ii) residual methods using the surface energy balance. These last methods calculate ET_d by subtracting sensible heat and soil heat fluxes from net radiation [17].

The following physical and empirical models based on the surface energy balance (SEB) approach are of interest: SEBI (Surface energy balance index) [18], TSM (Two-source model) [19] and ETMA (Evapotranspiration mapping algorithm) [20]. One of the most widely used models is METRIC (Mapping Evapotranspiration at high Resolution using Internalized Calibration) model [21], which is based almost entirely on the SEBAL model (Surface Energy Balance Algorithm for Land) developed by Bastiaanssen et al. [22]. Both models estimate crop ET_d, by solving the surface energy balance using spectral information from multispectral satellite images in the optical, near infrared and thermal ranges. Only remote sensing imagery that provides spectral information in the thermal band may be

Consuelo Gonzalo-Martín, Angel García-Pedrero and Ernestina Menasalvas: Center for Biomedical Technology, Universidad Politécnica de Madrid, Campus Montegancedo, Pozuelo de Alarcón 28233, Spain e-mail: consuelo.gonzalo@upm.es

Mario Lillo-Saavedra and Octavio Lagos: Faculty of Agricultural Engineering, University of Concepción, and Water Research Center for Agriculture and Mining, CRHIAM, University of Concepción, Chile

Manuscript received October, 2016; revised XXXX, 2016.

used as input to these models. Unfortunately, most of current operational remote sensors do not supply this information. Therefore, alternative methodologies that allow mapping ET_d, avoiding the need for a thermal band, should be researched for agricultural water management purposes. Machine learning methods for forecasting distributed ET_d on space and time are now becoming a promising area of research. In [23] is proposed an algorithm based on Wavelet Transform and Support Vector Machines that finds multiple relationships between input products (i.e. different satellite images) and output products (i.e. PNS MODIS or Latent Heat Flux (LE)) at different spatial scales. Even though the method has shown to achieve a good accuracy in the estimation of these products, the RMSE values obtained increases with the length of the forecast, and the method requires thermal information. In [24] a Relevance Vector Machine was trained with ET_d from METRIC to forecast the ET_d during days when Landsat images are not available. For this task, extrapolated temporal values of NDVI and LAI, reference evapotranspiration (ET_r) calculated from a weather station and thematic crop classes were used. These classes were generated through a supervised classification for each year studied, without considering the high variability of this kind of cover both from a spatial and temporal point of view.

Our work hypothesis states in which it is possible to train non-parametric models fed with values of NDVI and LAI spectral indexes, ET_r values of reference registered through a meteorological station and thematic classes, to generate a spatial distributed estimation of ET_d, without thermal spectral data.

The main goal of this paper is to evaluate the ability of Regression Random Forest Models (RRFM) to estimate spatially distributed ET_d for different thematic classes and dates where there is not a thermal band available to apply the surface energy balance models.

The training patterns of the RRFM have been characterized by features obtained from different dates and different land covers. Thus for each date, NDVI and LAI indexes, ET_r values obtained from a metereological station and a thematic map have been used as inputs to the RRFM. The thematic maps have been generated by the RUSboost algorithm and they have been included with the aim of considering agricultural land cover dynamics. Different sets of these features have been used to investigate and analyze the robustness, accuracy and general capability of the generated RRFM. The METRIC model output has been used as the target in the generation of the RRFM.

This paper is organized as follows. The theoretical description of the METRIC model, as well as, the machine learning methods used in this paper (RUSBoost classifier and Regression Random Forest) are presented in Section 2. The data sets used for the experimentation phase are described in Section 3. The methodology proposed is explained and illustrated in Section 4. The results are presented and discussed in Section 5. And Section 6 summarises the conclusions derived from the results.

II. Background

A. Surface Energy Balance Model: METRIC

METRIC is a satellite-based image-processing model for estimating ET_d based on algorithms which compute the surface energy balance components using remotely sensed surface reflectance in the visible and near-infrared wavebands and surface temperature (radiometric) from infrared thermal bands. Using this data and *in–situ* weather measurements, the instantaneous latent heat flux (LE, $W \cdot m^{-2}$) is calculated for each image pixel using a surface energy balance model (Eq. 1).

$$LE = R_n - G - H \tag{1}$$

Where R_n is net radiation ($W \cdot m^{-2}$), G is soil heat flux ($W \cdot m^{-2}$) and H is sensible heat flux ($W \cdot m^{-2}$). To compute the instantaneous soil heat fluxes G, an empirical relationship between leaf area index is used in accordance with [21]. R_n for each pixel, at the time of the satellite overpass, is estimated using the following equation:

$$R_n = (1-\alpha) \times R_{si} + R_{Li} - R_{Lr} - (1-\epsilon_0)R_{Li} \tag{2}$$

α representes the broadband surface albedo for each pixel, R_{si} the incoming shortwave solar radiation ($W \cdot m^{-2}$), R_{Li} and R_{Lr} are the incoming and outgoing longwave solar radiation respectively ($W \cdot m^{-2}$) and ϵ_0 represents the surface emissivity.

Instantaneous sensible heat fluxes are computed as:

$$H = \frac{\rho \times Cp \times dT}{r_{ah}} \tag{3}$$

Where ρ is the air density $(kg \cdot m^{-3})$; Cp the specific heat capacity of air $(1004 J \cdot kg^{-1} \cdot K^{-1})$; r_{ah} is the aerodynamic resistance to heat transport $(m \cdot s^{-1})$ and dT is the near surface air temperature gradient (K).

A relationship between the difference in temperature (dT) (at different heights) and surface temperature (T_s) for two extreme condition pixels, called anchor pixels (hot and cold pixels), is defined to estimate sensible heat fluxes. Thus, through Equation (4) it is possible to obtain the dT of each pixel for the whole image.

$$dT = b + a \times T_s \tag{4}$$

Coefficients a and b are obtained from anchor pixels using an iterative process proposed in [22] and modified in [21]. Subsequently, dT is used to estimate the sensible heat flux for each pixel.

The Fraction of the estimated evapotranspiration ($ETrF$) is obtained through equation (5). The ET_r is defined as the reference evapotranspiration calculated from data registered by a metereological station at the instant of the satellite image capture, and ET_{inst} is the instantaneous ET estimated from the METRIC model.

$$ET_rF = \frac{ET_{inst}}{ET_r} \tag{5}$$

Finally, it is possible to estimate the ET_d $(mm \cdot day^{-1})$ through ET_rF and the reference evapotranspiration for the daily period (ET_{r-d}) through Equation (6).

$$ET_d = ET_r \times ET_{r-d}F \tag{6}$$

A complete description of the METRIC model can be found in [21]. Figure 1 illustrates the whole process of the evapotranspiration estimation maps by METRIC.

One of the most critical parameters in the METRIC model are the anchor pixels. In the first approaches of these models [21], the selection of these parameters was made by an operator. But since the different criteria of these operators can be a source of error, automatic selection methods have been researched. In this work, the automatic method for the selection of anchor pixels proposed by [25] has been used.

B. RUSBoost classifier

To include information regarding the temporal variability of the agricultural covers to be analyzed in the models, a thematic map has been generated for each date through a supervised classification, using a RUSBoost classifier.

RUSBoost is a hybrid boosting/sampling method proposed by [26], which is a state-of-the-art method for learning from imbalanced datasets. RUSBoost improves the boosting algorithm by resampling training data in order to balance the class distribution. Unlike other ensemble methods, RUSBoost applies an under-sampling strategy to remove samples randomly from the majority class, before the training of each weak learner algorithm which is part of the ensemble.

Let $\mathbf{x}_i$ be a point in the feature space $\mathbf{X}$ and y_i be a class label in a set of class labels Y. Each of the examples in the data set ($\mathfrak{D}$) can be represented by the tuple $(\mathbf{x}_i, y_i)$. RUSBoost combines many weak classifiers h_t into a strong classifier H_{class} through linear combination. T weak learners are iteratively trained and added to the H_{class}. The final ensemble is constructed as:

$$H_{class}(\mathbf{x}) = \arg\max_{y \in Y} \sum_{t=1}^{T} h_t(\mathbf{x}, y) \log \frac{1}{\alpha_t} \tag{7}$$

where $H_{class}(\mathbf{x})$ is the prediction of the classifier H_{class} given the input feature vector $\mathbf{x}$, the resulting class $y \in Y$ is the one that gets the maximum value.

In each iteration t, RUSBoost randomly subsamples the majority class in training set $\mathfrak{D}_t$ until a subset $\mathfrak{D}'_t$ with a desired class distribution is reached. For example, if the desired class ratio r is 50:50, then the majority class examples are randomly removed until the numbers of the majority and minority class examples are equal. Hence a weight α_t is assigned to the weak learner according to the equation:

$$\alpha_t = \frac{\epsilon_t}{1 - \epsilon_t} \tag{8}$$

where ϵ_t represents the pseudo-loss based on the original training set $\mathfrak{D}_t$ and it is calculated as:

$$\epsilon_t = \sum_{(i,y): y_i \neq y} D_t(i)(1 - h_t(\mathbf{x}_i, y_i) + h_t(\mathbf{x}_i, y)) \tag{9}$$

where D_t represents the weight distribution, and $h_t(\mathbf{x}_i, y)$ the conditional probability of the class y given the feature vector $\mathbf{x}_i$. Initially, the weight of each example $D_1(i)$ is set to $\frac{1}{n}$, in which n is the number of examples in the training set. After each iteration, the weights are updated as follows:

$$D_{t+1}(i) = D_t(i) \alpha_t^{\frac{1}{2}(1 + h_t(\mathbf{x}_i, y_i) - h_t(\mathbf{x}_i, y: y \neq y_i))} \tag{10}$$

and then D_{t+1} is normalized to 1.

C. Regression Random Forest

A Regression Random Forest (RRF) is a predictor consisting of a collection of randomized base regression trees (weak predictors) $h_t(\mathbf{x}, \Theta_m)$, in which $m \geq 1$ and $\Theta_1, \ldots, \Theta_N$ are independent and identically distributed outputs of a random vector Θ [27], [28]. The output of these random trees are combined to form the aggregated regression estimated by equation 11.

$$H_{regress}(\mathbf{x}) = \frac{1}{T} \sum_{t=1}^{T} h_t(\mathbf{x}, \Theta), \tag{11}$$

in which $\mathbf{x} \in \mathfrak{D}_t$ and T represents the number of trees in the forest.

Unlike a classification problem, the output of the RRF takes on numerical values rather than class labels. The random vector Θ is used to determine how the successive cuts are made when building the individual trees and it is assumed to be independent of $\mathbf{x}$ and the training samples $\mathfrak{D}_t$ [27].

The generalization error for the RRFM depends on the strength of the individual trees in the forest and the correlation between them. This error, represented by the Euclidean distance $(Y - H_{regress}(\mathbf{X}))^2$, converges to a limit as the number of trees (T) in the forest becomes larger. A huge number of RRFM implementations can be found in the literature, which differ by 1) the way each individual tree is constructed, 2) the procedure used to generate the modified data sets on which each individual tree is constructed and 3) the way the predictions of each individual tree are aggregated to produce a unique consensus prediction [29].

Random Forest provides some key advantages against other well known classifiers: it has a non-parametric nature; it provides higher classification accuracy than other classical classifier, when the adequate attributes are considered for the characterization of the training patterns; and it is capable of determining the importance of the features [30]; moreover, it is robust against unbalanced classes distribution [31]. The aforementioned properties led us to choose Random Forest as the learning technique in this work. An ensemble of T decision trees for regression has been implemented by using the Statistics Toolbox from MATLAB ®.

III. Materials and Methods

A. Dataset description and pre-processing

The study site is located in the Central Valley in Chile, with central coordinates of 36^o $35'$ S and 72^o $00'$ W. The scene is composed of a city (Chillán), rivers, mainly different annual crops and orchards, and alluvial soils, which allows a high production for different crops. The climate is warm temperate, with an annual mean temperature of 14^o C, a short dry season and an annual rainfall ranging from 1,000 to 1,300 mm. Six images were captured by the ETM+ sensor on board the Landsat-7 satellite (path 233, row 85). They were downloaded from the USGS Glovis official site (http://glovis.usgs.gov), with an 1T preprocessing level of standard field correction.

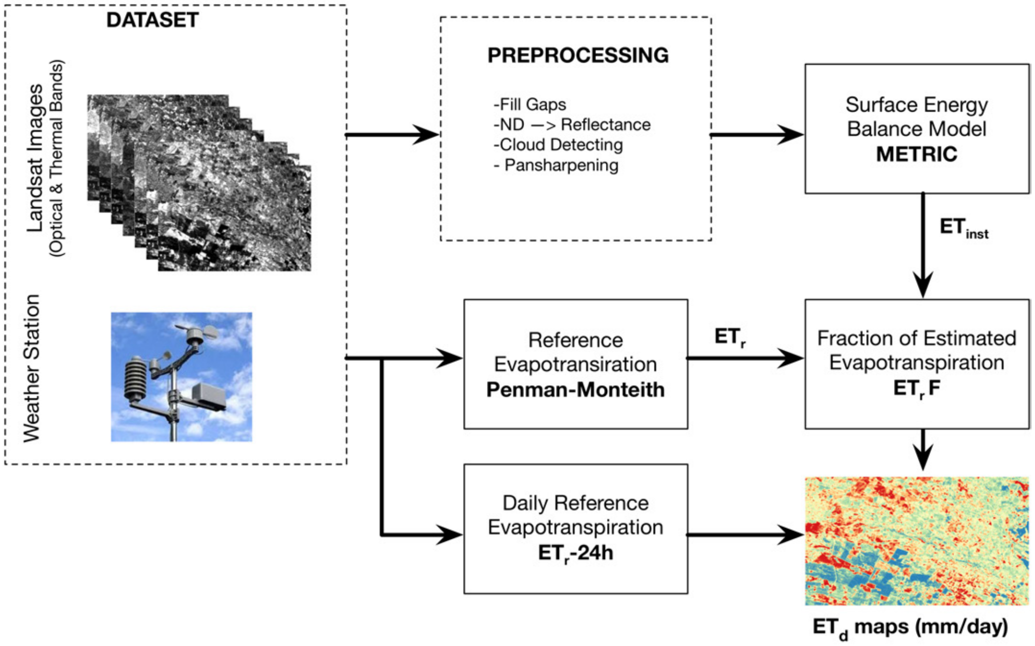

Fig. 1. Overview of the Evapotranspiration map estimation process.

Table I shows the details (dates and names) of the images from the summer season that have been used in this research. The label used to name each image is year–day in the Julian calendar. The size of the six Landsat-7 scenes is 947x702 pixels. Each pixel represents an area of 30 m x 30 m for all spectral bands, except for the thermal band. In this case each pixel represents an area of 60 m x 60 m. A RGB color composition of the image registered on 12 January 2012 is displayed in Figure 2. All images used have been preprocessed in order to ensure the quality of the data used for training the models. All outlier pixels with NaN and Inf values have been eliminated, also pixels with outlier ET_d values($ET_d < 0$ and $ET_d > 11 \ mm \cdot day^{-1}$) and the regions covered by clouds have been also eliminated. Four different land covers are presented in the scene: urban, agricultural vegetation, forest and bare soil.

Besides data obtained from the satellite images, other input data to the METRIC model were obtained from a meteorological station.

Data from an Eddy Covariance System (EC), an automatic weather station, as well as, crop evapotranspiration ET_c and reference evapotranspiration ET_o values have been used in this study to characterise the training patterns. The data registered by the EC are filtered considering only daily data and days without precipitation, and they have to fulfil the three following conditions: $R_n > LE$, $R_n > G$, $R_n > H$. Once the data have been filtered, further analysis splits into two parts. The first one calculates the mean of dairy latent fluxes of the following variables: sensible heat flux, soil heat flux, net radiation in a row and between rows (all of them in $W \cdot m^2$). The second part changes the unit of latent heat flux from $W \cdot m^2$ to $mm \cdot h^{-1}$. Regarding meteorological data only daily data are considered. Once crop ET_c and reference evapotranspiration ET_o are obtained, data from October to March of every season are analysed. This analysis corresponds to choose continuous days (at least three) where ET_c , ET_o, air temperature and net radiation are stable, without great variations. Once the days are selected, evapotranspiration ratio is calculated.

B. Methodology

In order to achieve the objetive established in the introduction, we propose a three-step methodology: i) generation of the RRFM; ii) validation of the models obtained to ensure the required precision; and iii) estimation of the ET_d maps only using optical information.

Figure 3 illustrates the workflow of the RRFM generation, as well as the evaluation of these models (steps i and ii). The raw meteorological and multispectral input data have been pre–processed eliminating the outliers data, and obtaining the input features used to train the RRFM. These input features are $\{NDVI_{map}, LAI_{map}, ET_r, CLASS_{map}\}$. ET_r being the reference evapotranspiration registered through a meteorological station. The values of the $CLASS_{map}$ feature are obtained through the aforementioned RUSBoost classifier. These values correspond to the four land covers identified in the study area: urban, agricultural vegetation, forest and bare soil.

TABLE I
LIST OF DATES USED IN THE STUDY. THE FIRST ROW SHOWS THE YEAR. THE SECOND ROW SHOWS MONTH/DAY. AND THE NAME OF EACH SCENE IS DISPLAYED IN THE THIRD ROW AS YEAR-JULIAN DAY.

Year	2012		2013	2014		2015
Date	01/12	01/28	01/31	02/02	18/02	05/02
Name	2012-012	2012-028	2013-031	2014-033	2014-049	2015-036

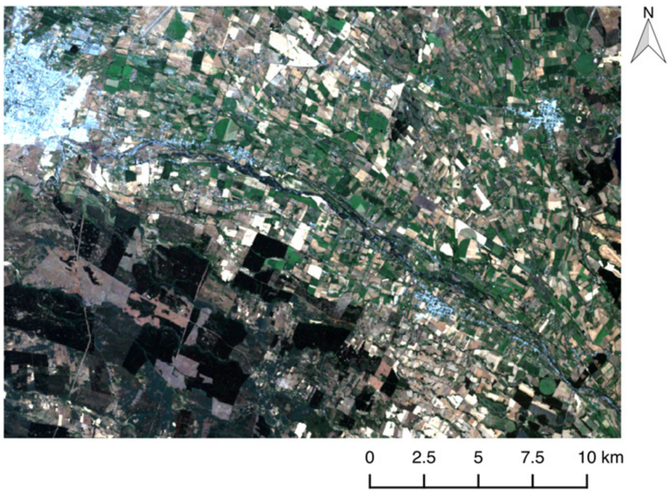

Fig. 2. RGB color composition of a Landsat-7 scene registered on 12 January 2012.

Each of the training set of values is associated with the corresponding daily evapotranspiration target value provided by METRIC (ET_{METRIC}).

To prove the suitability of the models for estimating the ET_d values from the seen data (data used to train the models) and the unseen data (real-world case), six different training datasets have been generated. These datasets have been built by removing a random date, which is used for testing. The remaining series of images is used for training the models.

A 10-fold cross validation has been used during the training phase. Once the models have been generated and evaluated through the calculation of the RMSE, the best model for each group of experiments is selected. The best model is defined as the one that obtains the minimum error in the validation set. This model is fed with the image that has not been used for the generation of the maps. Then, the evapotranspiration estimation errors are evaluated through the R-squared and the RMSE between the ET_d values estimated by METRIC (ET_d^{METRIC}) and the ET_d values estimated by the RRFM (ET_d^{RRFM}) for each thematic class and for each date being studied.

Details regarding how the data used by METRIC model has been registered as well as the ET_d^{METRIC} values obtained with our instruments are included in Annex I. In this annex also is included an analysis of the goodness of fit between METRIC and field measurements, as well as a fetch analysis of the EC station. The results of this analysis confirm the suitability of using METRIC as a reference.

Firstly, ET_d^{METRIC} and ET_d^{RRFM} values, for the whole image, have been calculated for each date and each thematic classes. A different scatterplot of ET_d^{METRIC} versus ET_d^{RRFM} has been presented for each date. And in each of them, the four considered thematic classes have been differenciated. The corresponding R-square values have been calculated. To analyze the performance of the values generated by the RRFM, the RMSE between the ET_d^{METRIC} and ET_d^{RRFM}, for each thematic class and for each date being studied, have been also calculated.

IV. RESULTS AND DISCUSSION

Figure 4 represents the scatterplots obtained by representing ET_d^{METRIC} against ET_d^{RRFM} for each date. In each scatterplot, the different thematic classes have been identified by a different color.

Now well, given the large number of pixels to be represented, four groups have been defined for each thematic class, based on the mean evapotranspiration value per group. Thus, each dot represents the mean evapotranspiration value of each one of the clusters defined for reasons of visualisation. The horizontal and vertical lines, associated to each dot, represent the deviation from the mean value produced by the ET_d^{METRIC} and ET_d^{RRFM}, respectively. It can be observed that for the land covers bare soil and urban areas, the deviation values for both models (METRIC and RRF) are larger than for agricultural vegetation and forest, but similar for both. On the other hand, it should be noted that the relation between RRFM with METRICS models is much more linear in these two last covers (agricultural vegetation and forest), areas of the special interest of this work, in particular agricultural vegetation.

The effect of the overestimation (dots above the diagonal) or underestimation (dots values under the diagonal) can be observed for all dates. These effects may be due to the difficulty in modelling non-linear natural phenomena considered in the METRIC model. A more profound analysis would be required to identify other variables that could improve the models in a more extended paper.

The R-squared values for each thematic class and each date corresponding to these scatterplots are included in Table II. The highest R-squared values, for each date, is shown in bold type, and the lowest value is shown in underlined type text. The values of this table corroborate the analysis on the scatterplots; and also show that the generated model provides the best estimation for agricultural vegetation, followed by forest land covers and urban areas and the worst for bare soil.

In order to evaluate the estimation quality depending on the date, the RMSE has been calculated for each class and for each date and the average values for each date have been obtained. Table III summarises the calculated RMSE

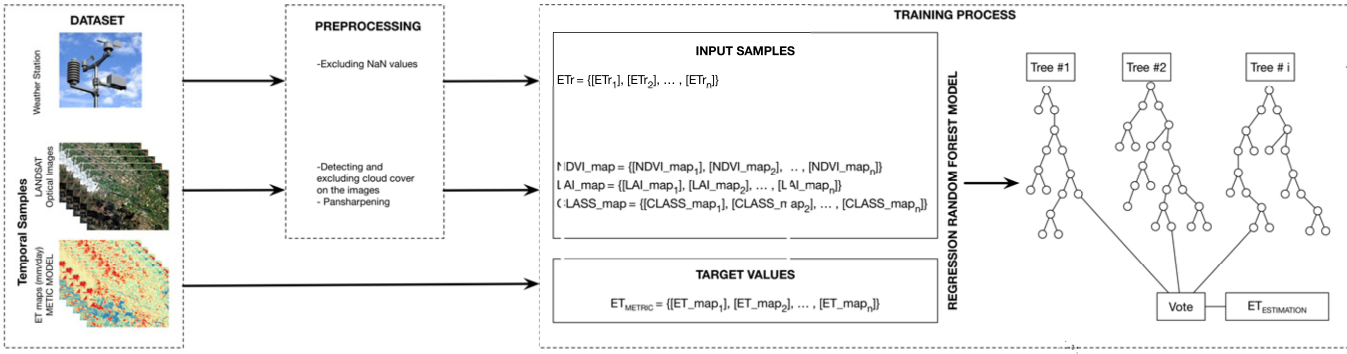

Fig. 3. Overview of the Regression Random Forest Model Generation.

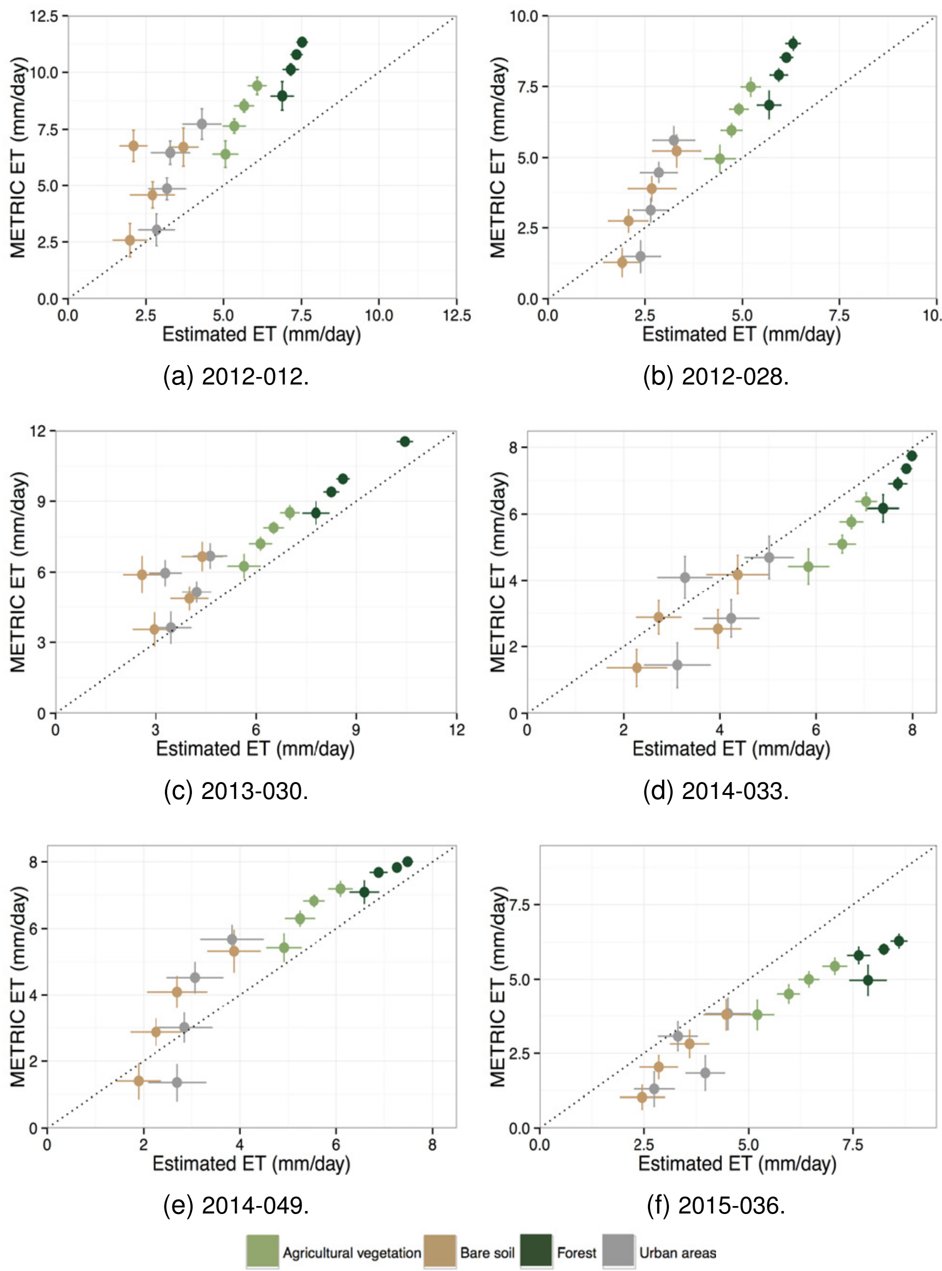

(a) 2012-012.

(b) 2012-028.

(c) 2013-030.

(d) 2014-033.

(e) 2014-049.

(f) 2015-036.

Fig. 4. Scatterplots of ET_d^{METRIC} against ET_d^{RRFM} for each of the dates analyzed.

TABLE II
R-SQUARED VALUES.

	2012-012	2012-028	2013-030	2014-033	2014-049	2015-036	Average
Urban areas	0.80	0.96	0.27	<u>0.38</u>	<u>0.80</u>	0.47	0.70
Agricultural vegetation	0.97	**0.99**	**0.99**	0.93	**0.90**	**0.99**	**0.96**
Forest	**0.99**	0.99	0.96	**0.99**	0.88	<u>0.42</u>	0.87
Bare soil	<u>0.26</u>	<u>0.93</u>	<u>0.16</u>	0.63	0.89	0.97	<u>0.64</u>

TABLE III
RMSE VALUES $(mm \cdot day^{-1})$.

	2012-012	2012-028	2013-030	2014-033	2014-049	2015-036	Average
Urban areas	**2.48**	1.53	1.75	<u>1.17</u>	<u>1.35</u>	1.33	1.60
Agricultural vegetation	2.57	1.60	1.20	<u>1.17</u>	1.03	1.49	1.51
Forest	<u>3.14</u>	<u>2.14</u>	**1.10**	**0.78**	**0.61**	<u>2.35</u>	1.68
Bare soil	2.94	**1.23**	<u>2.07</u>	0.86	1.08	**0.97**	1.52
Average (date)	<u>2.78</u>	1.62	1.53	**0.99**	1.05	1.53	

values. In this table, the values in bold represent the lowest values of RMSE for each date, while the highest values are underlined. It can be observed that the average RMSE is similar for most dates, with the exception of the 2012-012 and 2014-033. Analyzing the different factors that can justify this behavior, it should be noted that in the 2012-012 case, the maximum temperature was of $32°C$, slightly lower than the day before ($35°C$), moreover four days before (8^{th} February) the maximum precipitation of this month was registered (13.2 $mm{\cdot}day^{-1}$). While, in 2014-033 there were not precipitations in the days before and the maximum temperature was $24°C$. These two different situations have a strong influence in the selection of the anchor pixels, specially the cold pixel. Figure 5 shows the Evapotranspiration map provided by METRIC (Figure 5a) for the image 2012-012 and the corresponding Evapotranspiration map provided by the RRFM (Figure 5b). This dataset have been selected because according Table II and III, it presents the highest error for all considered datasets. The comparison between both maps allows appreciating a high similarity between them. It should be noted that, once again, the areas of higher difference correspond in the image with urban areas and bare soil. While the areas with lowest differences correspond with agricultural vegetation and forest.

To analyze the differences between METRIC and RRFM estimations for the particular case of agricultural vegetation landcover, a particular comparison has been carried out for the scene labeled 2012-012, restricted to this landcover. ET_d values larger than $(r\hat{m}s \pm \sigma)$ have been considered outliers and coloured in red; while values smaller than this threshold have been considered normal values and colored in green. All these points have been spatialised and superimposed on the thermal band of this scene (Figure 6). This visualisation allows observing that the outliers present a lower surface temperature (darker values in the scene) than the surrounding areas, which may be because outlier areas had recently been irrigated.

The proposed methodology presents the characteristic limitations of most regression models based on machine learning. All these models only can predict the values that they learn during the training phase. In this sense, it is critical that the training set includes the whole spectrum of the values that could be predicted. This kind of limitation is derived from the available training data.

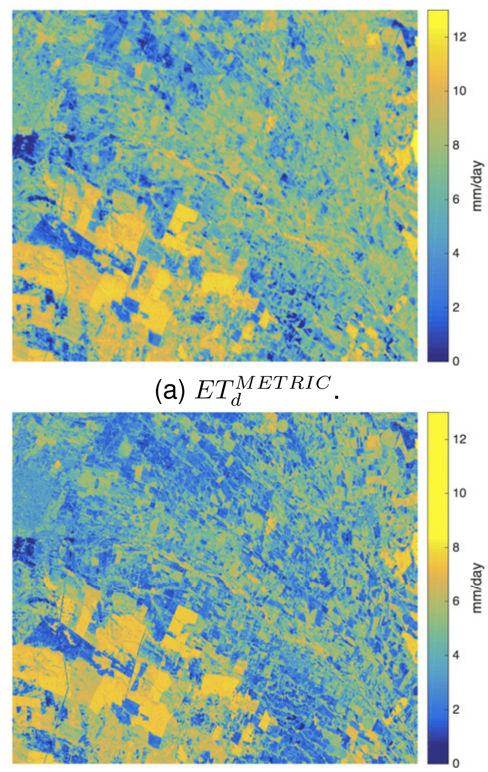

(a) ET_d^{METRIC}.

(b) ET_d^{RRFM}.

Fig. 5. Evapotranspiration maps, corresponding to a scene labeled 2012-012, obtained by METRIC (a) our RRFM (b).

V. Conclusion

The ultimate goal of this paper was to provide a model based on RRF that generates daily Evapotranspiration maps when there are not enough data to apply the SEB models. This goal has been achieved as it is shown by obtained results. It has been shown than the generated models by RRF present

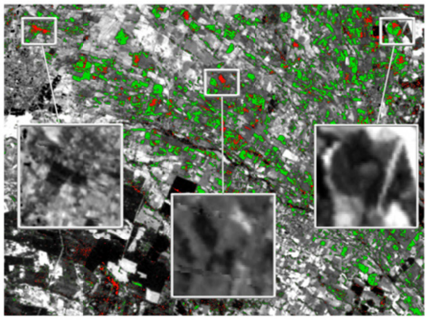

Fig. 6. Outliers superimposed on the thermal band of the scene.

a good agreement with METRIC models, especially for agricultural vegetation landcover ($overlineR - square = 0.96$) and forest ($\overline{R - square} = 0.87$). The spatially distributed visualisation of the evapotranspiration estimated by METRIC and RRFM shows a great similarity between both maps, since the areas of higher difference correspond with urban areas and bare soil; while the areas with lowest differences correspond with agricultural vegetation and forest. In other words, the generated RRFM are valid for green vegetation. However, it has been detected that the RRFM estimation quality depends on the meteorological conditions on the days previous to the satellite register. Since, METRIC is based on a balance of energy, it is able to detect this phenomenon, while RRFM is not able to detect this because it is mainly based on NDVI, and this index is completely altered by the presence of water in the covers. It can be concluded that the ET_d estimated by the RRFM would be feasible for real applications. Nevertheless, further investigations have to be done, mainly in applying other machine learning models, and integrating complementary information for the enrichment of the models.

ACKNOWLEDGMENT

A. García-Pedrero (grant 216146) acknowledges the support for the realization of his doctoral thesis to the Mexican National Council of Science and Technology (CONACyT). This work has been funded by Centro de Recursos Hídricos para la Agricultura y la Minería (CONICYT –FONDAP–1513001) and by Universidad Politécnica de Madrid (AL16–PID–07).

ANNEX I

First in this work, to evaluate ET_d values estimated by METRIC a field of 3.7 ha blueberry orchard, located at 36^o $37^{'}$ 15.67" S, 71^o $53^{'}$ 57.65" W, 125 m a.s.l. was considered. The soils in this site were formed from volcanic ashes (Andisols) with a silt loam texture. In 2006 blueberries, variety Legacy, were planted with a standard spacing of 1 m in a row and 3 m between rows. The selected area of the field has 3.333 plants per hectare, irrigated by a drip irrigation system, with 2 emitters per plant and a discharge of 2.2 $L \cdot h^{-1}$. An Eddy Covariance System was installed at this site to measure all energy balance components at 30-min intervals. To measure net radiation (over the crop row and between rows), two radiometers were used (NR-Lite2, Kipp & Zonen, Delft, the Netherlands). Soil heat fluxes were monitored by 4 plates (2 on the row and 2 between rows) (Huxseflux HFP01SC, Campbell Scientific, Logan, UT, USA) at 8 cm depth. Soil temperature was measured by 4 thermocouples for soil heat flux plate (TCAV, Campbell Scientific, Logan, UT, USA), positioned at 2, 4, 10 and 14 cm depth. The sensible heat was measured by a sonic anemometer 3D (CSAT3, Campbell Scientific, Logan, UT, USA) and by a fine wire thermocouple (FW3, Campbell Scientific, Logan, UT, USA). The latent heat was monitored using a sonic anemometer with a gas analyzer (EC150, Campbell Scientific, Logan, UT, USA). Air temperature and relative humidity were measured by an HMP45C probe (Campbell Scientific, Logan, UT, USA). The soil water content was monitored using an analog data logger (Em5b, Decagon Devices, Pullman, WA, USA), 2 sensors (EC- 5, Decagon Devices, Pullman, WA, USA) at 5 and 11 cm depth, 3 sensors (10HS, Decagon Devices, Pullman, WA, USA) at 20, 30, and 40 cm depth and 7 sensors (Watermark, Irrometer, Riverside, CA, USA), 4 of them at 10, 25, 40 and 55 cm depth on the row and 3 of them at 10, 25 and 40 cm depth between rows. Canopy temperature was monitored by an infrared radiometer (SI-400, Apogee Instruments, Logan, UT, USA), located at 2 m high and precipitation was measured by a rain gauge (Texas electronics TE525, Campbell Scientific, Logan, UT, USA). Then, with the aim of comparing the ET_d^{METRIC} obtained with our instruments into the blueberry orchard and values estimated in other published works, a footprint (source weight function) was calculated using the model proposed by [32]. The fetch for stable and unstable conditions as well as the Xpeak (Peak distance from measuring point to the maximum contributing source area (m) have been calculated. As shown in Figure 7 the analysis indicated that under unstable conditions 91% cumulative normalised flux measurements is obtained at nearly 150 m lengths. In order to analyse the reliability of measurements based on the EC system, energy balance closure was evaluated ((see Figure 8). The linear comparison between available energy ($Rn - G$) and turbulent energy fluxes ($H + LE$)) showed a slope of 0.83 and a coefficient of determination (R^2) of 0.98. To reduce the EC imbalance the Bowen ratio method for recalculating the turbulent energy fluxes was used.

Different surface energy balance models has been evaluated in the central irrigated valley of Chile to estimate ET_d from satellite images by several recent studies. In this area METRIC has been evaluated by [33] in sugarbeet, comparing ET estimations with measurements from a SEB system, by [34] in sugarbeet and cherry, and by [35] and [36] over a drip irrigated vineyard. Similarly, others surface energy balance models have been evaluated. [33] evaluates a surface energy balance model for partially vegetated surfaces over a sugarbeet field; [37] evaluated ET_d estimations over a drip-irrigated olive orchard by using thermal and multispectral cameras placed on a UAV; and [38] over a drip irrigated merlot vineyard. All evaluation showed that SEB models were able to estimate evapotranspiration from satellite images. In this study ET_d estimations with METRIC was compared with EC measurements, this analysis showed a RMSE value of $1.47 mm \cdot day^{-1}$ similar to previous studies.

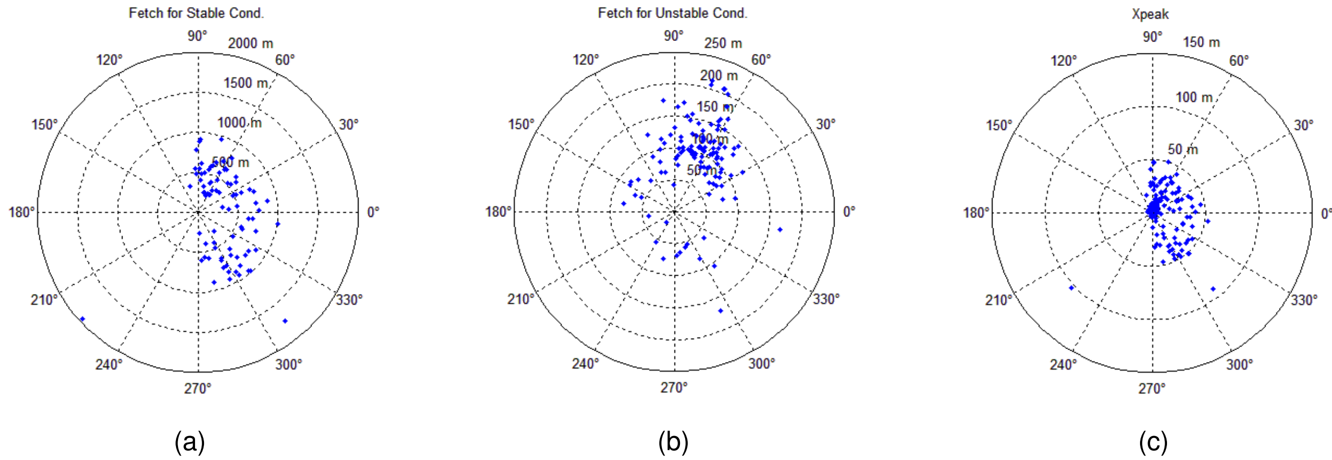

Fig. 7. Footprint analysis of Eddy Covariance measurements. a) Fetch for stable conditions. b) Fetch for unstable conditions. c) Xpeak.

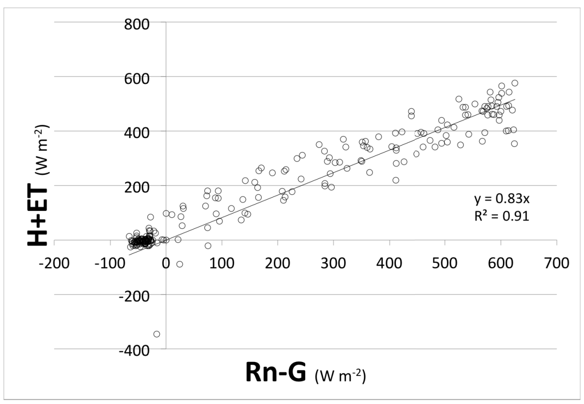

Fig. 8. Energy balance closure.

References

[1] X.-j. Wang, J.-y. Zhang, S. Shahid, E.-h. Guan, Y.-x. Wu, J. Gao, and R.-m. He, "Adaptation to climate change impacts on water demand," *Mitigation and Adaptation Strategies for Global Change*, vol. 21, no. 1, pp. 81–99, 2016.

[2] R. Snyder, C. Pedras, A. Montazar, J. Henry, and D. Ackley, "Advances in et-based landscape irrigation management," *Agricultural Water Management*, vol. 147, pp. 187–197, 2015.

[3] J. Jensen, J. L. Wright, and B. Pratt, "Estimating soil moisture depletion from climate, crop and soil data," *Transactions of the ASAE*, vol. 14, no. 6, pp. 954–959, 1971.

[4] R. Allen, L. Pereira, D. Raes, and M. Smith, *Crop Evapotranspiration: Guidelines for computing crop requirement, Irrigation and Drainage Paper No 56*. Rome, Italy: FAO, 1998.

[5] ASCE, *The ASCE Standardized equation for calculating reference evapotranspiration, Task Committee Report*. New York: Environment and Water Resources Institute of ASCE, 2002.

[6] J. Monteith, "Evaporation and the environment. symposium soc. expl. biol." vol. 19, 1965, pp. 205–234.

[7] D. I. Stannard, "Comparison of penman-monteith, shuttleworth-wallace, and modified priestley-taylor evapotranspiration models for wildland vegetation in semiarid rangeland," *Water Resources Research*, vol. 29, no. 5, pp. 1379–1392, 1993.

[8] I. Alves and L. Santos Pereira, "Modelling surface resistance from climatic variables?" *Agricultural Water Management*, vol. 42, no. 3, pp. 371–385, 2000.

[9] S. Ortega-Farias, A. Olioso, R. Antonioletti, and N. Brisson, "Evaluation of the penman-monteith model for estimating soybean evapotranspiration," *Irrigation Science*, vol. 23, no. 1, pp. 1–9, 2004.

[10] W. Shuttleworth, "Towards one-step estimation of crop water requirements," *Transactions of the ASAE*, vol. 49, no. 4, pp. 925–935, 2006.

[11] H. Flores, "Penman-monteith formulation for direct estimation of maize evapotranspiration in well watered conditions with full canopy," Ph.D. dissertation, University of Nebraska - Lincoln, 2007.

[12] S. Irmak, D. Mutiibwa, A. Irmak, T. Arkebauer, A. Weiss, D. Martin, and D. Eisenhauer, "On the scaling up leaf stomatal resistance to canopy resistance using photosynthetic photon flux density," *Agricultural and Forest Meteorology*, vol. 148, no. 6, pp. 1034–1044, 2008.

[13] W. Shuttleworth and J. Wallace, "Evaporation from sparse crops-an energy combination theory," *Quarterly Journal of the Royal Meteorological Society*, vol. 111, pp. 839–855, 1985.

[14] L. Jiang and S. Islam, "An intercomparison of regional latent heat flux estimation using remote sensing data," *Int. J. Remote Sens.*, vol. 24, no. 11, pp. 2221–2236, June 2003.

[15] R. R. Nemani and S. W. Running, "Estimation of regional surface resistance to evapotranspiration from ndvi and thermal-ir avhrr data," *J. Appl. Meteorol.*, vol. 28, no. 4, pp. 276–284, April 1989.

[16] R. R. Gillies, W. P. Kustas, and K. S. Humes, "A verification of the 'triangle' method for obtaining surface soil water content and energy fluxes from remote measurements of the normalized difference vegetation index (ndvi) and surface e," *International Journal of Remote Sensing*, vol. 18, no. 15, pp. 3145–3166, 1997. [Online]. Available: http://dx.doi.org/10.1080/014311697217026

[17] P. H. Gowda, J. L. Chavez, P. D. Colaizzi, S. R. Evett, T. A. Howell, and J. A. Tolk, "Et mapping for agricultural water management: present status and challenges," *Irrigation science*, vol. 26, no. 3, pp. 223–237, 2008.

[18] M. Meneti and B. Choudhary, "Parameterization of land surface evapotranspiration using a location dependent potential evapotranspiration and surface temperature range. exchange processes at the land surface for a range of space and time series, bolle, hj, feddes, ra, and kalma, jd," *International Association of Hydrological Sciences Publication*, vol. 212, pp. 561–568, 1993.

[19] W. Kustas and J. Norman, "Evaluation of soil and vegetation heat flux predictions using a simple two-source model with radiometric temperatures for partial canopy cover," *Agricultural and Forest Meteorology*, vol. 94, no. 1, pp. 13–29, 1999.

[20] S. Loheide and S. Gorelick, "A local-scale, high-resolution evapotranspiration mapping algorithm (etma) with hydroecological applications at riparian meadow restoration sites," *Remote Sensing of Environment*, vol. 98, no. 2, pp. 182–200, 2005.

[21] R. Allen, M. Tasumi, and R. Trezza, "Satellite-based energy balance for mapping evapotranspiration with internalized calibration (metric). model," *Journal of Irrigation and Drainage Engineering*, vol. 133, no. 4, pp. 380–394, 2007.

[22] W. Bastiaanssen, M. Meneti, R. Feddes, and A. Holtslag, "A remote sensing surface energy balance algorithm for land (sebal). formulation," *Journal of Hydrology*, vol. 212-213, pp. 198–212, 1998.

[23] Y. H. Kaheil, E. Rosero, M. K. Gill, M. McKee, and L. A. Bastidas, "Downscaling and forecasting of evapotranspiration using a synthetic model of wavelets and support vector machines," *IEEE Transactions on Geoscience and Remote Sensing*, vol. 46, no. 9, pp. 2692–2707, 2008.

[24] R. Bachour, W. R. Walker, A. M. Ticlavilca, M. McKee, and I. Maslova, “Estimation of Spatially Distributed Evapotranspiration Using Remote Sensing and a Relevance Vector Machine,” *Journal of Irrigation and Drainage Engineering*, vol. 140, no. 8, p. 04014029, Aug. 2014.

[25] R. G. Allen, B. Burnett, W. Kramber, J. Huntington, J. Kjaersgaard, A. Kilic, C. Kelly, and R. Trezza, “Automated calibration of the metric-landsat evapotranspiration process,” *JAWRA Journal of the American Water Resources Association*, vol. 49, no. 3, pp. 563–576, 2013. [Online]. Available: http://dx.doi.org/10.1111/jawr.12056

[26] C. Seiffert, T. M. Khoshgoftaar, J. Van Hulse, and A. Napolitano, “RUSBoost: A Hybrid Approach to Alleviating Class Imbalance,” *Systems, Man and Cybernetics, Part A: Systems and Humans, IEEE Transactions on*, vol. 40, no. 1, pp. 185–197, Jan. 2010.

[27] G. Biau, “Analysis of a random forests model,” *The Journal of Machine Learning Research*, vol. 13, no. 1, pp. 1063–1095, 2012.

[28] L. Breiman, “Random Forests,” *Machine Learning*, vol. 45, no. 1, pp. 5–32, 2001.

[29] J. S. K. J. Boulesteix, A. and I. Knig, “Overview of Random Forest Methodology and Practical Guidance with Emphasis on Computational Biology and Bioinformatics,” University of Munich, Department of Statistics, Tech. Rep., 2012.

[30] V. Rodriguez-Galiano, B. Ghimire, J. Rogan, M. Chica-Olmo, and J. Rigol-Sanchez, “An assessment of the effectiveness of a random forest classifier for land-cover classification,” *Journal of Photogrammetry and Remote Sensing*, vol. 67, pp. 93 – 104, 2012. [Online]. Available: http://www.sciencedirect.com/science/article/pii/S0924271611001304

[31] C. Chen, A. Liaw, and L. Breiman, “Using random forest to learn imbalanced data,” *University of California, Berkeley*, 2004.

[32] C. Hsieh, G. Katul, and T. Chi, “An approximate analytical model for footprint estimation of scalar fluxes in thermally stratified atmospheric flows,” *Advances in Water Resources*, vol. 23, no. 7, pp. 765–772, 2000.

[33] M. Aguirre, “Estimación de evapotranspiración en remolacha azucarera (beta vugaris) y componentes del balance de energía superficial usando seb-pv (the modified seb model for partially vegetated surfaces) e imágenes de satélite,” Magister, Facultad de Ingeniería Agrícola, Universidad de Concepción, Chile, 2017.

[34] D. Fonseca, “Estimación de evapotranspiración espacialmente distribuida mediante un enfoque geobia,” Ph.D., Facultad de Ingeniería Agrícola, Universidad de Concepción, Chile, 2017.

[35] M. Carrasco-Benavides, S. Ortega-Farías, L. Lagos, J. Kleissl, L. Morales, C. Poblete-Echeverría, and R. Allen, “Crop coefficients and actual evapotranspiration of a drip-irrigated merlot vineyard using multispectral satellite images,” *Irrigation Science*, vol. 30, no. 6, pp. 485–497, 2012.

[36] M. Carrasco-Benavides, S. Ortega-Farías, L. O. Lagos, J. Kleissl, L. Morales-Salinas, and A. Kilic, “Parameterization of the satellite-based model (metric) for the estimation of instantaneous surface energy balance components over a drip-irrigated vineyard,” *Remote Sensing*, vol. 6, no. 11, pp. 11 342–11 371, 2014.

[37] S. Ortega-Farías, S. Ortega-Salazar, T. Poblete, A. Kilic, R. Allen, C. Poblete-Echeverría, L. Ahumada-Orellana, M. Zuñiga, and D. Sepúlveda, “Estimation of energy balance components over a drip-irrigated olive orchard using thermal and multispectral cameras placed on a helicopter-based unmanned aerial vehicle (uav),” *Remote Sensing*, vol. 8, no. 8, p. 638, 2016.

[38] C. Poblete-Echeverría and S. Ortega-Farias, “Calibration and validation of a remote sensing algorithm to estimate energy balance components and daily actual evapotranspiration over a drip-irrigated merlot vineyard,” *Irrigation Science*, vol. 30, no. 6, pp. 537–553, 2012.

Consuelo Gonzalo–Martín received the Ph.D from the Complutense University of Madrid, in Physics, in 1989. Since 1991, she is working in the Computer School of Universidad Politécnica de Madrid. Since September 2012, she is doing her research activities at the Center for Biomedical Technology of the UPM. Her main contributions have been in the areas of image processing, and the development of new artificial neural networks algorithms in remote sensing, medical imaging and recognition of faces. At present, her main line of research is new methodologies for image analysis based on objects (OBIA) for satellite images and medical images. Also she is involved in text and image mining in the health care domain.

Mario Lillo–Saavedra received the B.E. degree in electrical engineering (1997) and M.Sc. (2001) from the University of Concepción, Chile, and Ph.D. degrees in Computer Sciences from the Technical University of Madrid (Spain, 2005). Since March 2000, he has been with the Faculty of Agricultural Engineering, at the University of Concepción, where he is Full Professor. His current research interests include object based image analysis (OBIA), remote sensing in agriculture, and machine learning. He is a member of the Water Research Center for Agriculture and Mining (CHRIAM) and Water Technology Research Laboratory for Agriculture ($ITecMA^2$), University of Concepción, Chile.

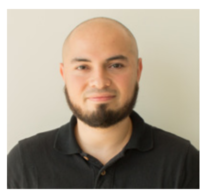

Angel Garca-Pedrero is a PhD student in the Advanced Computing for Science and Engineering at the Center for Biomedical Technology, Universidad Politcnica de Madrid (Spain). Prior to undertaking a PhD, he obtained a Master Degree in Computer Science, by the National Institute of Astrophysics, Optics and Electronics (Mexico) in 2009 and a Bachelor Degree in Computer Systems Engineering by the Villahermosa Institute of Technology (Mexico) in 2006. His research interests include object-based image analysis, image understanding and image interpretation (remotely sensed and medical images).

Ernestina Menasalva is Professor at the Department of Computer Systems Languages and Sw Engineering, Faculty of Computer Science of Universidad Politécnica de Madrid (UPM). She studied Computer Science and she has a PhD in Computer Science. She is nowadays member of MIDAS *Data Mining and data simulation group* at the Center of Biotechnology in UPM. Her research activities are on various aspects of data mining project development and in the last years her research is focused on data mining on the medical field.

Octavio Lagos received a B.E. (1997) and M.Sc. (2005) degrees in Agricultural Engineering from the University of Concepción-Chile, and a Ph.D. degree in Engineering from the University of Nebraska-Lincoln (USA, 2008). Since 2009, he has been with the faculty of Agricultural Engineering at the university of Concepción as an Associated Professor. His current research interests include Irrigation Engineering, Evapotranspiration Modelling and Measurements and Geographic Information Systems and Remote Sensing in Water Resources. He is member of the Water Resources Department, the Water research Center for Agriculture and Mining (CRHIAM) and the Water Technology Research Laboratory for Agriculture ($ITecMA^2$) at the University of Concepción Chile.